

The Activation Energy for Wall Slip

P. F. Pelz* and T. Corneli
Technische Universität Darmstadt
 (Dated: May 14, 2018)

The Navier slip boundary condition is interpreted as an equilibrium of shear rate and slip rate. From the argument that the slip rate shall be proportional to the molecules' collision rate, the temperature dependence of the Navier slip boundary condition is derived. The model for the temperature dependence of the slip length is validated by slip measurements of liquid hydrocarbons in a novel Couette type tribometer being introduced. The essence of the gained experimental data for one fluid-solid-interface is the quadruple activation energy for shear and wall slip together with the viscosity and slip length at a reference temperature. This quadruple is determined for four different hydrocarbon liquids of different molecular mass, structure and polarity proving the applicability of the new measurement method. From the executed systematic measurements three conclusions regarding the slip length dependence are pointed out: (i) the slip length increases with increasing molar mass; (ii) changing the molecular structure from saturated hydrocarbon to unsaturated affects the slip length as well as the activation energy for slip; (iii) adding a small fraction of polar molecules to the hydrocarbon decreases the slip length and increases the activation energy for wall slip due to the polar end-groups of the liquid.

During the past 20 years, different research groups measured slip at the interface of a fluid moving parallel to a solid; cf. review articles on boundary slip [1–3]. Understanding the molecular physics behind the slip condition is of importance for many fields of science: the transfer of momentum and matter as well as heterogeneous reactions in biological or technical systems are greatly influenced by the interface condition which is firstly formulated by Navier [4] in 1822.

Assessing the experimental investigations, it strikes that the temperature dependence of the Navier slip condition has been left out of the focus of most research on wall slip [5–34]. This is unexpected since the temperature dependence of a continuum mechanical property, e.g. the viscosity, gives an insight into the molecular constitution of matter. A prominent example for this is Einstein's work on Brownian motion [35]. From thermodynamics, kinetic theory or statistical mechanics the same rate equation

$$\frac{d \ln k}{dT} = \frac{E}{\mathcal{R}T^2} + \text{const.} \quad (1)$$

is derived, relating the rate k of a molecular process to the temperature T , activation energy E and gas constant \mathcal{R} [36]. With the temperature independent activation energy, the well known Arrhenius relation follows $k \propto \exp(-E/\mathcal{R}T)$ for the rate of the molecular process. Before applying and validating the Arrhenius relation for wall slip, and consequently determining the activation energy, we briefly review the experimental research on slip length measurements. This motivates the new Couette type slip length measuring device introduced here, being developed during the last five years, as a device where the surface averaged slip length is derived from an integral measure, i.e. the torque.

So far, the experimental research focuses either on verifying the existence of a wall slip or on influencing the effect by surfactants. Systematic investigations concentrate on the variation of shear rates. The suspected dependence of slip length on wall shear rate is still under discussion [17–21, 23, 37]. This might be due to mixing up measurement uncertainty and interpretation: the here presented measurements reveal no shear rate dependence of the slip length for hydrocarbon liquids moving relative to a metal surface up to a shear rate of the order of magnitude 10^5 s^{-1} in the temperature interval 12.5°C to 60.2°C .

The following liquid-solid-interface combinations are in the focus of research so far: water [5–8, 15–18, 20, 27–29, 37, 38], alkane [12–14, 16–19, 28, 29] or polymer melts [9, 11] moving relative to glass, mica, silicon [5–9, 17–23, 25–29, 39] or synthetic sapphire [11–14]. Technical most relevant is the hydrocarbon-metal-interface being here in focus. Keeping in mind, that roughly one third of primary energy is dissipated due to friction at this liquid-solid-interface [40–42] the relevance of the hydrocarbon-metal-interface becomes clear.

Until now, a systematic investigation of the temperature influence on the slip length aiming at the Arrhenius relation has not been pursued. Most of the slip length data are reported for only one temperature. Only Churaev et al. [43] and Fetzer et al. [44, 45] measure slip lengths at different temperatures. First steps are made in simulating the molecular dynamics at the interface [46, 47]: although the dimensionless temperature is varied, the experimental validation of the simulation is still pending, since length and energy scales of the molecules are so far unknown. In this light, the presented results may contribute in determining some of the unknown scales for future molecular dynamic simulations. Churaev et al. [43] measure the slip length of water moving relative to solid glass in the temperature range from 2°C to 35°C . Fetzer et al. [44, 45] measure the slip length of an amorphous

* peter.pelz@fst.tu-darmstadt.de

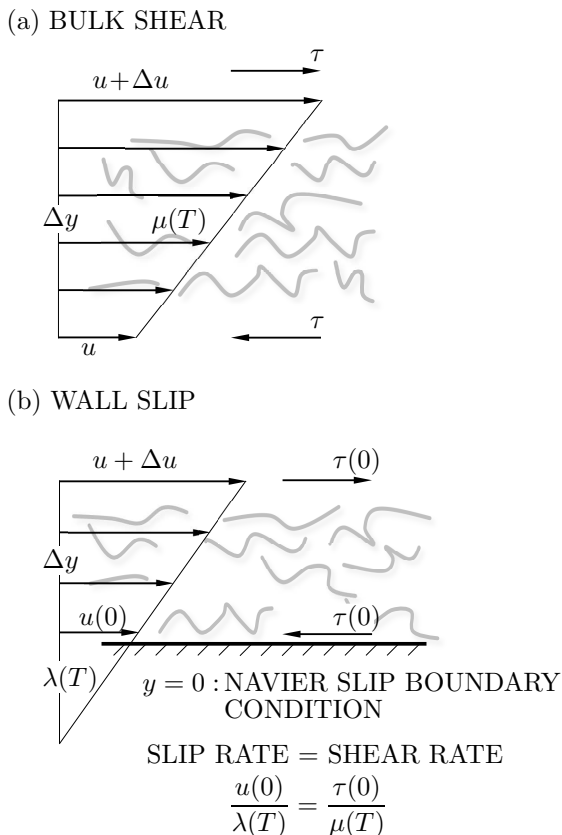


FIG. 1. Schemata of bulk shear (a) and wall slip (b) for molecules sliding relative to each other and relative to a solid wall.

liquid polymer melt moving relative to a coated silicon solid. The temperature ranges from 105 °C to 130 °C, i.e. close to the glass transition temperature of the polymer. Both measurements reveal a decreasing slip length with increasing temperature. Fetzer et al. fit a power law for the temperature dependent friction coefficient without gaining further physical insight.

Within this letter we address five novel findings to the physics at the interface of a liquid and a solid wall: (i) by arguments based on dimensional analysis and the collision model we derive an Arrhenius relation for the temperature dependence of the slip length; (ii) we present a novel Couette type tribometer being developed over the last five years to measure wall slip at various temperatures; (iii) the presented experiments reveal no shear rate dependence of the slip length up to a shear rate of the order of magnitude 10^5 s^{-1} in the temperature interval 12.5 °C to 60.2 °C; (iv) the Arrhenius relation for the temperature dependence of the slip length is experimentally validated for four hydrocarbon liquids of different molecular masses and the activation energy for wall slip is derived for all four interfaces; (v) the influence of molecular weight, structure and polarity of the fluid on the slip length and activation energy is discussed.

In the following paragraph we motivate the Arrhenius

relation for wall slip from collision theory. Shear and slip at a solid wall are related by the Navier slip boundary condition: although this boundary condition is often seen as a kinematic relation, Navier himself has interpreted it in the year 1822 as a dynamic relation [4]. As will be seen, this original view indeed leads to deeper insight. Figure 1 shows schematically (a) bulk shear deformation and (b) wall slip of molecules at homogeneous temperature T . At equilibrium the near wall molecules adhere to the wall, $y = 0$, as well as to each other. In the ensemble average the electrostatic molecular forces sum up to a shear stress τ being a macroscopic or continuum mechanical quantity such as dynamic viscosity $\mu(T)$. At non-equilibrium the molecules slide (in the time average) relative to each other and relative to the wall. $u(y)$ denotes the ensemble averaged velocity parallel to the wall at the wall normal distance y .

Applying a shear stress τ to a Newtonian fluid at constant temperature T results in a shear deformation of constant rate $\partial u / \partial y = \tau / \mu(T)$. The molecular counterpart to this ensemble averaged macroscopic rate is the collision rate of the molecules $k_\mu(T) \propto \exp(-E_\mu / \mathcal{R}T)$ (activation energy E_μ , general gas constant \mathcal{R}). For reasons of dimensions, i.e. due to the Bridgman's postulate [48], both rates shall be linear dependent resulting in $\tau / \mu(T) \propto \exp(-E_\mu / \mathcal{R}T)$ (cf. the argumentation of Truesdell [49]). Hence, the well known temperature dependence of viscosity of a liquid $\mu(T) \propto \exp(E_\mu / \mathcal{R}T)$ is on hand. The logarithm of the ratio of $\mu(T)$ and $\mu_0 = \mu(T_0)$ defines the time-temperature-shift factor

$$a_\mu := \log \frac{\mu(T)}{\mu(T_0)} = \frac{E_\mu}{\mathcal{R}} \left(\frac{1}{T} - \frac{1}{T_0} \right). \quad (2)$$

With this in mind, the expectation and motivation for the research presented here is the following: there should be an Arrhenius relation such as (2) and hence an activation energy E_λ for wall slip as well. Based on Navier's work, Helmholtz [50] introduced in 1860 the slip length $\lambda(T)$ as the ratio of slip velocity and velocity gradient $u(0) / (\partial u / \partial y)|_{y=0}$. Thus, besides the shear rate $\tau / \mu(T)$, there is a second ensemble averaged macroscopic rate, the slip rate $u(0) / \lambda(T)$. The molecular counterpart to this rate is the collision rate of molecules at the interface $k_\lambda \propto \exp(-E_\lambda / \mathcal{R}T)$, being different from k_μ . The slip rate and k_λ are linear dependent due to reasons of dimensions resulting in $u(0) / \lambda(T) \propto \exp(-E_\lambda / \mathcal{R}T)$. Hence, we derive the temperature dependence of the slip length of a liquid $\lambda(T) \propto \exp(E_\lambda / \mathcal{R}T)$. It is expected, that the activation energy for wall slip E_λ differs from the activation energy E_μ for bulk shear. The logarithm of the ratio of $\lambda(T)$ and $\lambda_0 = \lambda(T_0)$ defines again a time-temperature-shift factor

$$a_\lambda := \log \frac{\lambda(T)}{\lambda(T_0)} = \frac{E_\lambda}{\mathcal{R}} \left(\frac{1}{T} - \frac{1}{T_0} \right), \quad (3)$$

but now for wall slip. In conclusion, the viscous momen-

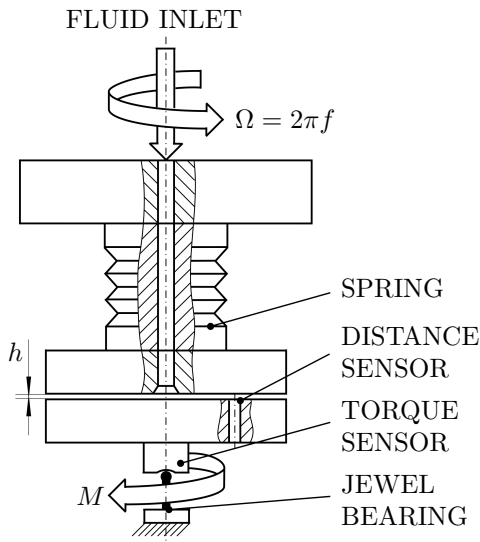


FIG. 2. Principle sketch of the slip length tribometer (disk diameter is 64 mm). The temperature is controlled by tempering the tribometer as well as the fluid in a temperature test chamber.

tum transport for one fluid-solid-interface is fully determined by the provided quadruple $[\mu(T_0), E_\mu, \lambda(T_0), E_\lambda]$. Equivalent to $\lambda(T)$, sometimes the ratio $k(T) := \lambda(T)/\mu(T) = u(0)/\tau$ is used cf. [44, 46, 47]. This so called friction factor of course follows an Arrhenius relation as well, showing the activation energy $E_k = E_\lambda - E_\mu$. The quadruple $[\mu(T_0), E_\mu, \lambda(T_0), E_\lambda]$ and $[\mu(T_0), E_\mu, k(T_0), E_k]$ are equivalent; with one given quadruple the other one can be derived by the given transformation.

In the light of the above discussion, it is indeed beneficial interpreting the Navier slip boundary condition as a dynamic equilibrium of the two rates, i.e. slip rate and shear rate:

$$\frac{u(0)}{\lambda(T)} = \frac{\tau(0)}{\mu(T)} \quad (\text{at the wall}). \quad (4)$$

With (2) and (3) the temperature dependence of this dynamic Navier slip boundary condition is expected to follow the relation

$$\log \frac{\tau(0)}{\mu_0} \frac{\lambda_0}{u(0)} = \frac{a_\mu(T, T_0)}{a_\lambda(T, T_0)} = \frac{E_\mu - E_\lambda}{\mathcal{R}} \left(\frac{1}{T} - \frac{1}{T_0} \right). \quad (5)$$

To validate the Arrhenius relation for wall slip, we introduce a new integral method for measuring the bulk viscosity $\mu(T)$ and wall slip $\lambda(T)$ as a function of the fluid temperature T at once. The apparatus schematically shown in figure 2 is the slip length tribometer developed over the last five years by the authors: the upper disk rotates with constant rotational speed $\Omega = 2\pi f$ relative to the lower one. Both circular disks ($\varnothing 64$ mm) are made of

an edge hardened stainless steel (steel type 1.8519). The planarity of both disks is smaller than ± 15 nm and the arithmetic mean roughness is below 10 nm. The transmitted torque M is measured at the support of the lower disk. The gap height h is measured by means of a capacitive distance sensors with a resolution of 4 nm.

To allow a cardanic self levelling of the two disks relative to each other, the lower one is supported by a jewel bearing. The gap height h is controlled by means of the fluid pressure at the fluid inlet. The pressure forces the fluid radial outward. At the same time the fluid is sheared in the circumferential direction. The circumferential Couette velocity profile is $u(r, y) = \Omega r (y + \lambda) / (h + 2\lambda)$ (radius r , axial coordinate $0 < y < h$). For small gap height h the nonlinear convective acceleration is negligible and the equation of motion is linear. Hence, the circumferential Couette velocity profile is independent from the radial velocity profile. Thus, for the laminar flow the inverse torque is gained as

$$M^{-1} = \frac{h + 2\lambda}{\mu \Omega I_P}, \quad (6)$$

with the polar second moment of area $I_P := \int_A r^2 dA$ of the disks.

The relation (6) shows that the inverse torque M^{-1} is proportional to the apparent gap height $h + 2\lambda$. M^{-1} is linear in h . For the no-slip boundary condition, i.e. vanishing slip length $\lambda \rightarrow 0$, the inverse torque $M^{-1} \rightarrow 0$ for $h \rightarrow 0$. For non-vanishing slip length $\lambda > 0$ the $M^{-1} - h$ - curve is shifted to the left. The intersection with the axis of abscissa equals two times the slip length λ (cf. fig. 3). It is not possible to reach $h \rightarrow 0$ due to two reasons: first, due to micro roughness a solid-solid contact would not be avoidable; second, M would tend to infinity as h approaches zero. But this is no drawback: the conceptional design of the device is such, that λ is gained from the extrapolation of the line relation $h \rightarrow 0$. Figure 3 shows the result of typical experiments at constant temperature of $T = (313.15 \pm 0.1)$ K, i.e. at $\Theta = (40 \pm 0.1)$ °C. Clearly the linear behaviour of the inverse frictional torque M^{-1} reveals. The coefficient of determination for equation (6) is above 0.999. Based on this linearity of the inverse torque, the earlier mentioned shear rate independence of the slip length is asserted: all measurements plotted in Fig. 3 show the same slip length, even though the shear rate varies from $2 \cdot 10^3 \text{ s}^{-1}$ to $2 \cdot 10^5 \text{ s}^{-1}$. The measured mean slip length for synthetic hydrocarbon alpha-olefin (PAO 6) at 40 °C is $\lambda = 475$ nm (for a detailed uncertainty quantification the reader is referred to the supplementary material of this letter).

Figure 4 shows the Arrhenius plot for the time-temperature-shift factors (2), (3) for bulk shear $a_\mu(T, T_0)$ and wall slip $a_\lambda(T, T_0)$: both factors are plotted versus the inverse absolute temperature T . As expected, both relations (2) and (3) are observed validating the model. The energy barrier for bulk shear of the alpha-olefin is $E_\mu = 33.5 \text{ kJ mol}^{-1}$. New is the

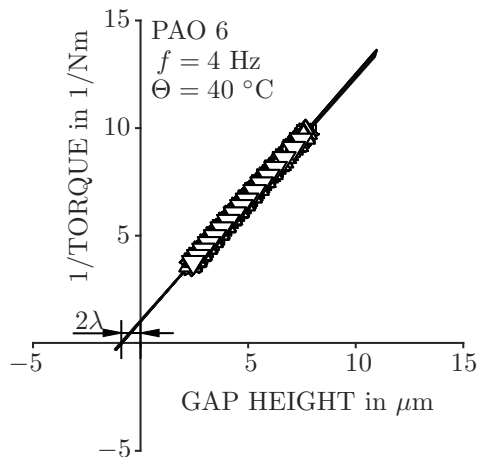


FIG. 3. Result of a typical experiment at $\Theta = 40$ °C and constant rotational speed of 4 Hz for a synthetic hydrocarbon alpha-olefin (PAO 6). The figure shows 42 measurement runs. Each run is marked by a symbol. Only the last one marked by triangles is visible.

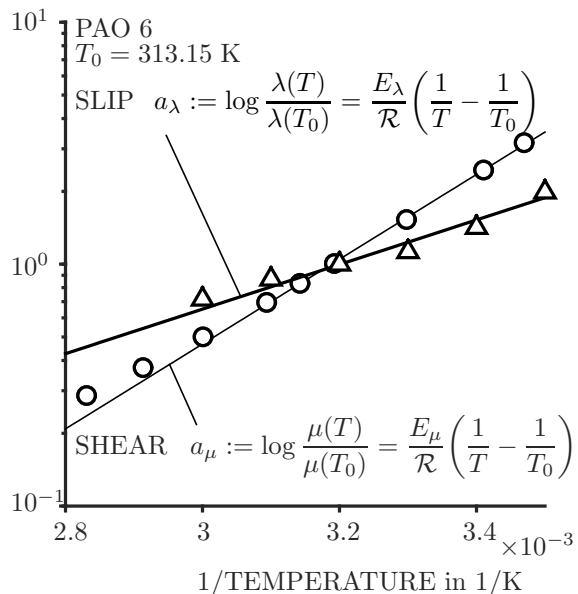


FIG. 4. Arrhenius plot for bulk shear and wall slip for the alpha-olefin. The activation energy for bulk shear is $E_\mu = 33.5$ kJ mol⁻¹ and for wall slip $E_\lambda = 17.6$ kJ mol⁻¹.

so far unknown activation energy for slip relative to lipophilic metal surface: the experiments indicate an activation energy of $E_\lambda = 17.6$ kJ mol⁻¹.

The activation energy for bulk shear and wall slip shall both depend on the van der Waals forces and hence on two major factors: first on the molecule's length, i.e. the geometric mean average of the molar mass \bar{M} ; second on the polarity of the molecules.

To validate this hypotheses, we varied the molecular structure from the unsaturated hydrocarbon alpha-olefin, being a blend of three main fractions (cf. Fig. 5), to two saturated hydrocarbons, i.e. mineral oils of mean molar mass $\bar{M} = 666$ u (ISO VG 46) and 806 u (ISO VG 68). Finally we added a small fraction of long chained molecules with polar end-groups (viscosity index improver, VI) to the mineral oil (ISO VG 46). Adding a small fraction of long chained molecules changes the viscosity as well as the activation energy for bulk shearing. The fraction of the added molecules was such selected that the viscosity of the modified mineral oil (ISO VG 46+VI) at 40 °C corresponds to the viscosity of the mineral oil ISO VG 68 at the same temperature. Table I gives the quadruple $[\mu(T_0), E_\mu, \lambda(T_0), E_\lambda]$, describing the tribological system hydrocarbon-metal-interface for each fluid. From the results we point out three conclusions regarding the dependence of the slip length and activation energy for slip: (i) the slip length increases with increasing molar mass; (ii) a change from saturated (eq. ISO VG 68) to unsaturated (eq. PAO 6) hydrocarbon influences both shear and slip; (iii) adding a small fraction of polar molecules to the hydrocarbon decreases the slip length and increases the activation energy for wall slip due to the polar end-groups of the liquid. Assessing the unpolar hydrocarbon molecules, there is an increase in slip length with increasing molecular mass.

TABLE I. The table gives the quadruple $[\mu(T_0), E_\mu, \lambda(T_0), E_\lambda]$ for each of the four investigated fluids.

Fluid	\bar{M} in u	$\mu(T_0)$ in mPas	E_μ in kJ mol ⁻¹	$\lambda(T_0)$ in nm	E_λ in kJ mol ⁻¹
ISO VG 46	666	38.4	41.3	120	23.7
ISO VG 68	806	58.1	45.0	143	26.7
PAO 6	882	25.8	33.5	468	17.6
ISO VG 46 + VI	666	58.1	40.3	65	43.0

[1] C. Neto, D. R. Evans, E. Bonaccorso, H.-J. Butt, and V. S. J. Craig, Boundary slip in newtonian liquids: a review of experimental studies,

Reports on Progress in Physics **68**, 2859 (2005).

[2] E. Lauga, M. Brenner, and H. Stone, Microfluidics: The no-slip boundary condition, in

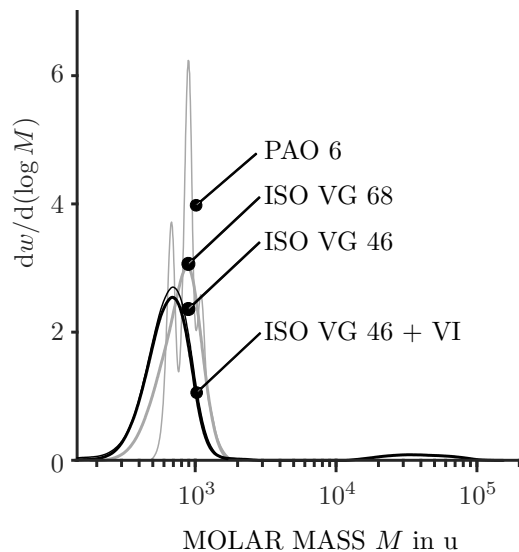


FIG. 5. Area normalized molar mass distribution for the alpha-olefin (PAO 6), the mineral oils (ISO VG 46, ISO VG 68) as well as for the mineral oil modified by a small fraction of long chained molecules with polar end-groups (ISO VG 46 + VI).

Springer Handbook of Experimental Fluid Mechanics, edited by C. Tropea, A. L. Yarin, and J. F. Foss (Springer Berlin Heidelberg, Berlin, Heidelberg, 2007) pp. 1219–1240.

- [3] B.-Y. Cao, J. Sun, M. Chen, and Z.-Y. Guo, Molecular momentum transport at fluid-solid interfaces in mems/nems: A review, *Journal of Molecular Sciences* **10**, 4638–4706 (2009).
- [4] M. Navier, Sur les lois du mouvement des fluides, *Mémoires de l'Academie royal des Sciences de l'Institut de France* **27**, 414 (1822).
- [5] C. D. Meinhart, S. T. Wereley, and J. G. Santiago, Piv measurements of a microchannel flow, *Experiments in Fluids* **27**, 414 (1999).
- [6] D. C. Tretheway and C. D. Meinhart, Apparent fluid slip at hydrophobic microchannel walls, *Physics of Fluids* **14**, L9 (2002).
- [7] P. Joseph and P. Tabeling, Direct measurement of the apparent slip length, *Physical Review E* **71**, 035303 (2005).
- [8] P. Joseph, C. Cottin-Bizonne, J. M. Benoit, C. Ybert, C. Journet, P. Tabeling, and L. Bocquet, Slippage of water past superhydrophobic carbon nanotube forests in microchannels, *Phys. Rev. Lett.* **97**, 156104 (2006).
- [9] L. Léger, H. Hervet, G. Massey, and E. Durliat, Wall slip in polymer melts, *Journal of Physics: Condensed Matter* **9**, 7719 (1997).
- [10] L. Léger, H. Hervet, and R. Pit, Interfacial properties on the submicrometer scale (American Chemical Society, 2000) Book section Friction and Flow with Slip at Fluid-Solid Interfaces, pp. 154–167.
- [11] L. Léger, Friction mechanisms and interfacial slip at fluid-solid interfaces, *Journal of Physics: Condensed Matter* **15**, S19 (2003).
- [12] R. Pit, H. Hervet, and L. Léger, Friction and slip of a simple liquid at a solid surface, *Tribology Letters* **7**, 147 (1999).
- [13] R. Pit, H. Hervet, and L. Léger, Direct experimental evidence of slip in hexadecane: Solid interfaces, *Phys. Rev. Lett.* **85**, 980 (2000).
- [14] T. Schmatko, H. Hervet, and L. Léger, Friction and slip at simple fluid-solid interfaces: The roles of the molecular shape and the solid-liquid interaction, *Phys. Rev. Lett.* **94**, 244501 (2005).
- [15] K. Watanabe, Y. Udagawa, and H. Udagawa, Drag reduction of newtonian fluid in a circular pipe with a highly water-repellent wall, *Journal of Fluid Mechanics* **381**, 225 (1999).
- [16] J. T. Cheng and N. Giordano, Fluid flow through nanometer-scale channels, *Physical Review E* **65**, 031206 (2002).
- [17] Y. Zhu and S. Granick, Rate-dependent slip of newtonian liquid at smooth surfaces, *Phys. Rev. Lett.* **87**, 096105 (2001).
- [18] Y. Zhu and S. Granick, Apparent slip of newtonian fluids past adsorbed polymer layers, *Macromolecules* **35**, 4658 (2002).
- [19] Y. Zhu and S. Granick, No-slip boundary condition switches to partial slip when fluid contains surfactant, *Langmuir* **18**, 10058 (2002).
- [20] Y. Zhu and S. Granick, Limits of the hydrodynamic no-slip boundary condition, *Phys. Rev. Lett.* **88**, 106102 (2002).
- [21] E. Bonaccorso, H.-J. Butt, and V. S. J. Craig, Surface roughness and hydrodynamic boundary slip of a newtonian fluid in a completely wetting system, *Phys. Rev. Lett.* **90**, 144501 (2003).
- [22] E. Bonaccorso, M. Kappl, and H.-J. Butt, Hydrodynamic force measurements: boundary slip of water on hydrophilic surfaces and electrokinetic effects, *Phys. Rev. Lett.* **88**, 076103 (2002).
- [23] V. S. J. Craig, C. Neto, and D. R. M. Williams, Shear-dependent boundary slip in an aqueous newtonian liquid, *Phys. Rev. Lett.* **87**, 054504 (2001).
- [24] S. Ecke, R. Raiteri, E. Bonaccorso, C. Reiner, H.-J. Butt, and V. S. J. Craig, Measuring normal and friction forces acting on individual fine particles, *Review of Scientific Instruments* **72**, 4164 (2001).
- [25] O. I. Vinogradova and G. E. Yakubov, Dynamic effects on force measurements. 2. lubrication and the atomic force microscope, *Langmuir* **19**, 1227 (2003).
- [26] F. Restagno, J. Crassous, I. Charlaix, C. Cottin-Bizonne, and M. Monchanin, A new surface forces apparatus for nanorheology, *Review of Scientific Instruments* **73**, 2292 (2002).
- [27] C. Cottin-Bizonne, S. Jurine, J. Baudry, J. Crassous, F. Restagno, and I. Charlaix, É, Nanorheology: An investigation of the boundary condition at hydrophobic and hydrophilic interfaces, *The European Physical Journal E* **9**, 47 (2002).
- [28] C. Cottin-Bizonne, B. Cross, A. Steinberger, and E. Charlaix, Boundary slip on smooth hydrophobic surfaces: Intrinsic effects and possible artifacts, *Phys. Rev. Lett.* **94**, 056102 (2005).
- [29] C. Cottin-Bizonne, A. Steinberger, B. Cross, O. Racourt, and E. Charlaix, Nanohydrodynamics: The intrinsic flow boundary condition on smooth surfaces, *Langmuir* **24**, 1165 (2008).
- [30] C. Neto, V. Craig, and D. Williams, Evidence of shear-dependent boundary slip in newtonian liquids, *Eur. Phys. J. E* **12**, 71 (2003).

- [31] C. L. Henry, C. Neto, D. R. Evans, S. Biggs, and V. S. J. Craig, The effect of surfactant adsorption on liquid boundary slippage, *Physica A: Statistical Mechanics and its Applications* **339**, 60 (2004).
- [32] J.-H. J. Cho, B. M. Law, and F. Rieutord, Dipole-dependent slip of newtonian liquids at smooth solid hydrophobic surfaces, *Phys. Rev. Lett.* **92**, 166102 (2004).
- [33] R. Truesdell, A. Mammoli, P. Vorobieff, F. van Swol, and C. J. Brinker, Drag reduction on a patterned superhydrophobic surface, *Physical Review Letters* **97**, 044504 (2006).
- [34] C. Cheikh and G. Koper, Stick-slip transition at the nanometer scale, *Phys. Rev. Lett.* **91**, 156102 (2003).
- [35] A. Einstein, Über die von der molekularkinetischen theorie der wärme geforderte bewegung von in ruhenden flüssigkeiten suspendierten teilchen, *Annalen der Physik* **322**, 12 (1905).
- [36] K. J. Laidler and M. C. King, Development of transition-state theory, *The Journal of Physical Chemistry* **87**, 2657 (1983).
- [37] C.-H. Choi, K. J. A. Westin, and K. S. Breuer, Apparent slip flows in hydrophilic and hydrophobic microchannels, *Physics of Fluids* **15**, 2897 (2003).
- [38] D. Lumma, A. Best, A. Gansen, F. Feuillebois, J. O. Rädler, and O. I. Vinogradova, Flow profile near a wall measured by double-focus fluorescence cross-correlation, *Phys. Rev. E* **67**, 056313 (2003).
- [39] P. Huang, J. S. Guasto, and K. S. Breuer, Direct measurement of slip velocities using three-dimensional total internal reflection velocimetry, *Journal of Fluid Mechanics* **566**, 447 (2006).
- [40] J. Spurk, *Dimensionsanalyse in der Strömungslehre* (Springer Berlin Heidelberg, 1992).
- [41] K. Holmberg, P. Andersson, and A. Erdemir, Global energy consumption due to friction in passenger cars, *Tribology International* **47**, 221 (2012).
- [42] K. Holmberg, P. Andersson, N.-O. Nylund, K. Mäkelä, and A. Erdemir, Global energy consumption due to friction in trucks and buses, *Tribology International* **78**, 94 (2014).
- [43] N. V. Churaev, V. D. Sobolev, and A. N. Somov, Slippage of liquids over lyophobic solid surfaces, *Journal of Colloid and Interface Science* **97**, 574 (1984).
- [44] R. Fetzer, M. Rauscher, A. Münch, B. A. Wagner, and K. Jacobs, Slip-controlled thin-film dynamics, *EPL (Europhysics Letters)* **75**, 638 (2006).
- [45] R. Fetzer, A. Münch, B. Wagner, M. Rauscher, and K. Jacobs, Quantifying hydrodynamic slip: A comprehensive analysis of dewetting profiles, *Langmuir* **23**, 10559 (2007).
- [46] M. Müller, C. Pastorino, and J. Servantie, Flow, slippage and a hydrodynamic boundary condition of polymers at surfaces, *Journal of Physics: Condensed Matter* **20**, 494225 (2008).
- [47] J. Servantie and M. Müller, Temperature dependence of the slip length in polymer melts at attractive surfaces, *Physical Review Letters* **101**, 026101 (2008).
- [48] P. Bridgman, *Dimensional Analysis* (Yale University Press, 1922).
- [49] C. Truesdell, On the viscosity of fluids according to the kinetic theory, *Zeitschrift für Physik* **131**, 273 (1952).
- [50] H. Helmholtz and G. von Piotrowski, Über reibung tropfbarer flüssigkeiten, *Sitzungsberichte der Kaiserlichen Akademie der Wissenschaften. Mathematisch-Naturwissenschaftliche Classe* **40**, 607 (1860).
- [51] H. Hervet and L. Léger, Flow with slip at the wall: from simple to complex fluids, *Comptes Rendus Physique* **4**, 241 (2003).
- [52] J. L. Poiseuille, *Comptes rendus 11, Mémoires des Savants Etrangers* 9 (1840).
- [53] O. I. Vinogradova, Drainage of a thin liquid film confined between hydrophobic surfaces, *Langmuir* **11**, 2213 (1995).
- [54] W. Kamke, *Der Umgang mit experimentellen Daten, insbesondere Fehleranalyse, im physikalischen Anfänger-Praktikum: Eine elementare Einführung* (Selbstverl., 2010).

**SUPPLEMENTARY MATERIAL FOR "THE
ACTIVATION ENERGY FOR WALL SLIP":
UNCERTAINTY QUANTIFICATION**

In this supplementary material for the letter "The Activation Energy for Wall Slip" we provide a rigorous uncertainty quantification for the measurement data gained with the novel Couette type tribometer being introduced. The presented uncertainty quantification leads to the confidence interval for the slip length λ , i.e. $\delta\lambda_{95\%} = \pm 91.4 \text{ nm}$ and the uncertainty of the measurement system $\delta\lambda = \pm 33.2 \text{ nm}$.

The slip length tribometer is based on the linear relation (cf. Eq. (6) of the letter)

$$M^{-1} = \frac{h+2\lambda}{\mu\Omega I_P} \quad \text{or} \quad y = a + bx, \quad (7)$$

mapping the distance $x = h$ on the inverse torque $y = M^{-1}$. In the experiment, the gap height h and the frictional torque M are the directly and simultaneously measured quantities. The indirect measured quantities are the sum of the slip length 2λ at both interfaces, given by the zero point of the linear equation (cf. Fig. 3 of the letter) and the viscosity μ . Provided a and b are unknown, the slip length is obtained by

$$\lambda = \frac{1}{2} \frac{a}{b}. \quad (8)$$

The viscosity is

$$\mu = \frac{1}{b\Omega I_P}. \quad (9)$$

The intercept

$$a = \frac{\sum x_i^2 \sum y_i - \sum x_i \sum x_i y_i}{n \sum x_i^2 - (\sum x_i)^2}, \quad i = 1, \dots, n, \quad (10)$$

and the slope

$$b = \frac{n \sum x_i y_i - \sum x_i \sum y_i}{n \sum x_i^2 - (\sum x_i)^2}, \quad i = 1, \dots, n, \quad (11)$$

of Eq. (7) are determined by means of a least square fit for the n measured data. Since both measurands, the distance x and the inverse torque y , are subjected to a systematic and statistical measurement uncertainty, intercept a and the slope b are uncertain as well. The square of the uncertainty regarding the slip length (cf. Eq. (8)) is given by the Gaussian uncertainty propagation

$$(\delta\lambda)^2 = \left(\frac{\partial\lambda}{\partial a}\right)^2 (\delta a)^2 + \left(\frac{\partial\lambda}{\partial b}\right)^2 (\delta b)^2 \quad (12)$$

$$= \left(\frac{1}{2b}\right)^2 (\delta a)^2 + \left(\frac{a}{2b^2}\right)^2 (\delta b)^2. \quad (13)$$

Eq. (13) considers the uncertainty of the intercept δa as well as the uncertainty of the slope δb . Both uncertainties are unknown so far. The uncertainties of intercept and slope are determined using the generalized Gaussian uncertainty quantification. Both direct measurands show a mean \bar{x}, \bar{y} , a statistical uncertainty s (empirical standard deviation) and systematic uncertainty $\delta x, \delta y$ (cf. Fig. 6). In the experiment x and y are independent measurands. Thus, with respect to correlated uncertainty, only the systematic measurement uncertainties have to be taken into account as correlated uncertainties. The uncertainty of intercept δa and slope δb are then given by the following expressions:

$$\begin{aligned} (\delta a)^2 = & \sum_{i=1}^n \left[(\delta x)^2 \left(\frac{\partial a}{\partial x_i}\right)^2 + [s^2 + (\delta y)^2] \left(\frac{\partial a}{\partial y_i}\right)^2 \right] + (14) \\ & + 2 \sum_{i=1}^{n-1} \sum_{k=i+1}^n \left[(\delta x)^2 \left(\frac{\partial a}{\partial x_i}\right) \left(\frac{\partial a}{\partial x_k}\right) + \right. \\ & \left. + (\delta y)^2 \left(\frac{\partial a}{\partial y_i}\right) \left(\frac{\partial a}{\partial y_k}\right) \right], \end{aligned}$$

$$\begin{aligned} (\delta b)^2 = & \sum_{i=1}^n \left[(\delta x)^2 \left(\frac{\partial b}{\partial x_i}\right)^2 + [s^2 + (\delta y)^2] \left(\frac{\partial b}{\partial y_i}\right)^2 \right] + (15) \\ & + 2 \sum_{i=1}^{n-1} \sum_{k=i+1}^n \left[(\delta x)^2 \left(\frac{\partial b}{\partial x_i}\right) \left(\frac{\partial b}{\partial x_k}\right) + \right. \\ & \left. + (\delta y)^2 \left(\frac{\partial b}{\partial y_i}\right) \left(\frac{\partial b}{\partial y_k}\right) \right]. \end{aligned}$$

The partial derivatives are given for $i, j = 1, \dots, n$ by

$$\frac{\partial a}{\partial x_i} = \frac{2x_i \sum y_j - (\sum x_j y_j + y_i \sum x_j)}{n \sum x_j^2 - (\sum x_j)^2} + \quad (16)$$

$$- 2 \frac{(\sum x_j^2 \sum y_j - \sum x_j \sum x_j y_j) (nx_i - \sum x_j)}{(n \sum x_j^2 - (\sum x_j)^2)^2},$$

$$\frac{\partial a}{\partial y_i} = \frac{\sum x_j^2 - x_i \sum x_j}{n \sum x_j^2 - (\sum x_j)^2}, \quad (17)$$

$$\frac{\partial b}{\partial x_i} = \frac{n y_i - \sum y_j}{n \sum x_j^2 - (\sum x_j)^2} + \quad (18)$$

$$- 2 \frac{(n \sum x_j y_j - \sum x_j \sum y_j) (nx_i - \sum x_j)}{(n \sum x_j^2 - (\sum x_j)^2)^2},$$

$$\frac{\partial b}{\partial y_i} = \frac{nx_i - \sum x_j}{n \sum x_j^2 - (\sum x_j)^2}. \quad (19)$$

Still the statistical uncertainty s (empirical standard deviation) and systematic uncertainties δx and δy have to be considered. The origin of these uncertainties as well as their quantification are explained step by step in the following section.

The empirical variance

$$s^2 = \frac{1}{n-1} \sum_{i=1}^n \left[M_i^{-1} - (a + bx_i) \right]^2 \quad (20)$$

takes the statistical uncertainty of the measurands (x_i, y_i) from the linear relation $y = a + bx$ into account. This statistical uncertainty is reduced by repeating the experiment m times. We perform $m = 20 \dots 40$ measurement series to reduce $(\delta\lambda)^2$. Each measurement series consists of $p = 15 \dots 20$ measuring points, cf. Fig. 6. The evaluation of the linear regression is based on the measuring points of all m measurement series. Hence, the linear regression is supported by $n = m * p = 300 \dots 800$ measuring points for one single slip length measurement only. This results in a variance $s^2 \approx 0.0015 (\text{Nm})^{-2}$ for Eq. (20). In addition, each measuring point is averaged over 70,000 individual measurements in a measurement interval of 10 seconds. As a result of this averaging process, the variances of the single measuring points can be neglected compared to the deviations of the linear relation. The measurement time per measurement series to obtain the slip length is approximately 45 minutes. On average, 30 series of measurements are recorded for each temperature dependent slip length in the Arrhenius plot (cf. Fig. 4 of the letter).

The systematic uncertainty δy of the inverse torque results from the nonlinearity of the torque measuring system. Since we measure the torque and not the inverse torque, the uncertainty of the inverse torque is determined again by means of Gaussian uncertainty propagation

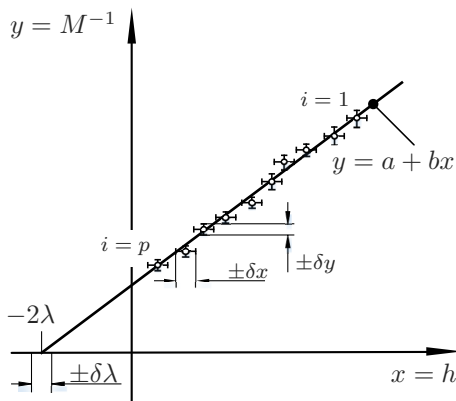


FIG. 6. Statistical and systematic uncertainties for measuring the slip length.

$$\delta y = \frac{1}{M^2} \delta M. \quad (21)$$

The systematic uncertainty of the torque measurement is composed of the uncertainty of the sensor and the signal processor and is specified by an uncertainty bound

$\delta M = 0.7 \text{ mNm}$. An uncertainty bound corresponds to a uniform distribution of the uncertainty. For the Gaussian uncertainty propagation, the uncertainty shall be normal distributed. Hence, the uniform distributed uncertainty of the uncertainty bound is converted into a normal distributed uncertainty

$$\delta y = \frac{1}{\sqrt{3}} \frac{\delta M}{M^2}, \quad (22)$$

cf. Kamke [54].

The systematic uncertainty δx of the distance measurement results from two sources: (i) the calibration of the capacitive distance sensor $\delta x_S = 60 \text{ nm}$, and (ii) the planarity of the disks $\delta x_D = 30 \text{ nm}$. The total uncertainty of the distance measurement results from the addition of both partial uncertainties $\delta x = 90 \text{ nm}$.

We are now in a position for determining the total measurement uncertainty of the slip length measurement in two steps: (i) first the statistical, s , and the systematic measurement uncertainties, δx , δy , are inserted into equations (14) and (15), determining the uncertainty of intercept δa and slope δb ; (ii) second, the calculated uncertainty of intercept δa and slope δb are inserted in Eq. (13) giving the uncertainty of the slip length measurement $\delta\lambda$.

For the measurement presented in Fig. 3 of the letter the uncertainty amounts for $\delta\lambda = 46.6 \text{ nm}$. Considering a 95% confidence interval the slip length is measured with an uncertainty of $\delta\lambda_{95\%} = \pm 91.4 \text{ nm}$.

Reported uncertainties for slip length measurements vary of the order of magnitude 1 nm to 10^3 nm . Cottin-Bizonne et al. [28] measure the slip length with an uncertainty below 10 nm for atomically smooth surfaces. The reported uncertainty by Pit et al. [13] is 50 nm for their experiments. The reported uncertainty by Fetzer et al. [44, 45] varies between $50 \dots 3000 \text{ nm}$.

Our uncertainty consideration takes the uncertainty of the probe as well as the uncertainty of the measurement system into account, since the uncertainty $\delta x_D = 30 \text{ nm}$ is related to the manufacturing tolerance of the metal surfaces. Excluding this uncertainty, the uncertainty of the measurement system yields $\delta\lambda = 33.2 \text{ nm}$. This uncertainty is relevant for comparing the tribometer as a measurement system with measurement systems measuring the slip length of atomically smooth surfaces.

In conclusion, the introduced novel Couette typ tribometer is indeed reliable and competitive for measuring the temperature-dependent slip length of atomically smooth as well as of rough surfaces.

ACKNOWLEDGMENTS

The authors thank Johannes Emmert and Professor Andreas Dreizler, both Technische Universität Darmstadt for the fruitful discussion leading to this uncertainty quantification.